iScience

CellPress
OPEN ACCESS

Article

# Terahertz spectral properties of glucose and two disaccharides in solid and liquid states

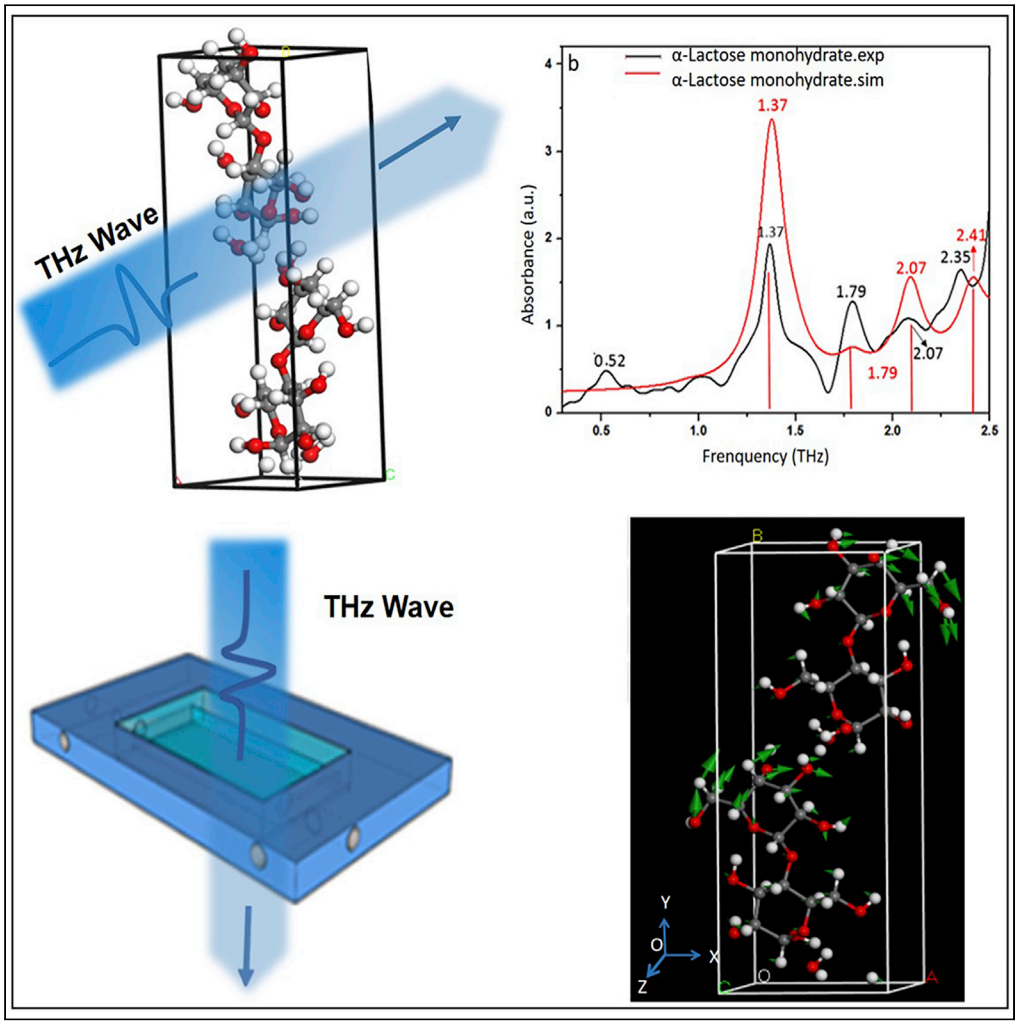


Haiyun Huang, Siyu Shao, Guoyang Wang, Ping Ye, Bo Su, Cunlin Zhang

subo75@cnu.edu.cn

## Highlights

Solid D-glucose, α-lactose hydrate, and β-maltose hydrate have unique absorption peaks

The simulated results of the three saccharides are consistent with the experimental ones

The THz spectra of the three saccharides in solid and aqueous solutions are correlated

Huang et al., iScience *25*, 104102
April 15, 2022 
https://doi.org/10.1016/j.isci.2022.104102

iScience

CellPress
OPEN ACCESS

Article

# Terahertz spectral properties of glucose and two disaccharides in solid and liquid states

Haiyun Huang,[1,2,3,4] Siyu Shao,[1,2,3,4] Guoyang Wang,[1,2,3,4] Ping Ye,[4] Bo Su,[1,2,3,4,5,*] and Cunlin Zhang[1,2,3,4]

## SUMMARY

**The vibrational and rotational frequencies of most biological macromolecules fall within the terahertz (THz) band; therefore, the THz wave has a strong ability to distinguish substances. Saccharides are important organic substances and the main source of life-sustaining activities. In this study, the spectral characteristics of D-glucose, α-lactose hydrate, and β-maltose hydrate were measured in the solid state through THz time-domain spectroscopy in the frequency range of 0.1–2.5 THz. The crystal configurations of these three saccharides were then simulated using solid-state density functional theory, and the experimental results were found to be in good agreement with the simulation results. Furthermore, the spectral characteristics of the three saccharides in solutions were measured. Each saccharide was found to have unique spectral characteristics, and a correlation existed between the THz absorption spectra of the same substance in the solid state and aqueous solution.**

## INTRODUCTION

The terahertz (THz) band refers to frequencies in the range of 0.1–10 THz and wavelengths in the range of 30 μm–3 mm. THz waves coincide with millimeter waves in the longwave band and infrared light in the shortwave band. In addition, THz waves are not only the transition zone from the macroscopic classical theory to the microscopic quantum theory but also the transition zone from electronics to photonics, which is referred to as the "THz gap" of the electromagnetic spectrum (Han et al., 2010). Several studies have found that most of the vibrational and rotational modes of biological macromolecules are in the THz band; therefore, THz technology provides a theoretical basis for biological sample recognition (Li et al., 2014; Nishizawa et al., 2008; Banh et al., 2006; Kumar et al., 2013; Walther et al., 2010. THz time-domain spectroscopy (THz-TDS) is a representative technique of THz spectroscopy, which can be used to effectively obtain the physical and chemical information of materials. In addition, the low energy of THz photons does not damage the measured substance. Therefore, the THz technology is a very useful nondestructive detection technology. In recent years, considerable advances have been made in the application of THz spectroscopy to the field of biomedical detection. The quantitative diagnosis of pathological tissues through the analysis of optical parameters has become a new research focus of biomedical photonics (Clothier and Bourne, 2003; Liu et al., 2018). The analysis of saccharides has always been the focus in biomedical research. Saccharides participate in the composition of human tissues in the form of proteoglycans, glycoproteins, and glycolipids. In addition, some glycoproteins have specific biological functions, such as cell-to-cell messaging, cellular immunity, and cell recognition (Calegari et al., 2017; Sahud et al., 2013; Liu et al., 2013; Mclellan et al., 2013; Selvarajan and Mohanasrinivasan, 2015; Sahud et al., 2013, 2013). D-Glucose is a type of polyhydroxyaldehyde, which is the most widely distributed and important monosaccharide in nature. Maltose is a colorless crystal; it is a disaccharide formed by the dehydration of two glucose molecules connected by glycosidic bonds. Maltose usually contains a crystal water molecule. Lactose is a typical disaccharide formed by the condensation of glucose and galactose; it usually crystallizes with a molecule of water to form α-lactose hydrate. D-Glucose, α-lactose hydrate, and β-maltose hydrate have similar molecular structure and contain a large number of hydrogen bonds, and we hope to know more about their spectral characteristics in the THz band (Klein et al., 1996; Zheng et al., 2012; Whiteside et al., 2008). It is known that different saccharides have different spectral absorptions in the THz band and even isomers of the same saccharides have different spectral characteristics. Upadhya et al. measured the high-resolution absorption spectra of different polycrystalline sugars in the 0.1- to 3-THz range and determined the vibrational characteristics of the absorption peaks using simulations (Upadhya et al., 2004). In the present study, we not only measured the absorption spectra of D-glucose, α-lactose hydrate, and β-maltose hydrate in the solid state via a transmission THz-TDS

[1]Key Laboratory of Terahertz Optoelectronics, Ministry of Education, Beijing 100048, China

[2]Beijing Key Laboratory for Terahertz Spectroscopy and Imaging, Beijing 100048, China

[3]Beijing Advanced Innovation Centre for Imaging Theory and Technology, Beijing 100048, China

[4]Department of Physics, Capital Normal University, Beijing 100048, China

[5]Lead contact

*Correspondence: subo75@cnu.edu.cn

https://doi.org/10.1016/j.isci.2022.104102

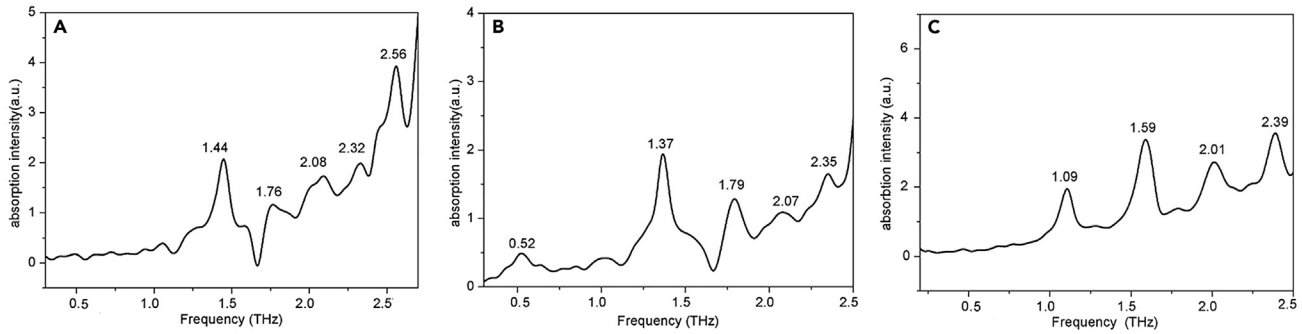


**Figure 1. THz transmission absorption spectra of solid D-glucose, solid α-lactose hydrate, and solid β-maltose hydrate**

(A) Solid D-glucose.

(B) Solid α-lactose hydrate.

(C) Solid β-maltose hydrate.

system but also simulated their intermolecular vibration modes using the solid-state density functional theory (DFT) software. Furthermore, we prepared a THz microfluidic chip and measured the spectral characteristics of the three saccharides in the solution state. We found that the THz spectra of the same saccharides in the solid state and aqueous solution were strongly correlated.

## RESULTS AND DISCUSSION

### THz spectra of the three solid saccharides

The solid tablet samples of the three saccharides were measured via THz-TDS system. The THz absorption spectra are shown in Figure 1. As shown in Figure 1A, solid D-glucose has characteristic absorption peaks at 1.44, 1.76, 2.08, 2.32, and 2.56 THz, and the peak positions are roughly the same as those of the solid glucose reported by Wang et al. (2016). As shown in Figure 1B, solid α-lactose hydrate has characteristic absorption peaks at 0.52, 1.37, 1.79, 2.07, and 2.35 THz. Finally, as shown in Figure 1C, solid β-maltose hydrate has characteristic absorption peaks at 1.09, 1.59, 2.01, and 2.39 THz.

### Simulation of the three solid saccharides

The shape and size of crystal cell can be expressed using six parameters, namely the lattice characteristic parameters, including the lengths of three groups of edges (i.e., the axial length of the crystal) *a*, *b*, and *c* of the crystal cell and the angle between the three groups of edges (i.e., the axial angle of the crystal) $\alpha$, $\beta$, and $\gamma$, of which, $\alpha = c \wedge b$, $\beta = a \wedge c$, $\gamma = a \wedge b$. The crystal cell structure of D-glucose, which is orthogonal and has the $P2_12_12_1$ (19) chiral space group, is shown in Figure 2A, and its structural parameters are $a$ = 9.714 (11) Å, $b$ = 14.99 (2) Å, $c$ = 4.262 (19) Å, $\alpha = 90°$, $\beta = 90°$, and $\gamma = 90°$. The simulation results and experimental absorption characteristics in the THz band of D-glucose are shown in Figure 2B; it can be seen that the simulated absorption peaks are consistent with the experimental ones. However, there are some offsets and discrepancies between the simulation and experimental results. The simulation is based on the fully idealized crystal structure and was conducted at 0 K, whereas the experiment was conducted at 300 K. The thermal motion between molecules may result in the displacement of the absorption peak. The different vibrational modes of D-glucose in the THz band are shown in Figures 2C–2F. The experimental absorption peak at 1.44 THz corresponds to the simulated absorption peak at 1.41 THz; this peak mainly originates from the intermolecular interaction and collective vibration of D-glucose molecules, as shown in Figure 2C. The experimental absorption peak at 1.76 THz corresponds to the simulated absorption peak at 1.72 THz; this peak is generated due to the rotation of the six-membered ring as well as the wagging of −CHOH and −OH, as shown in Figure 2D. The experimental absorption peak at 2.08 THz corresponds to the simulated absorption peak at 2.12 THz; this peak predominantly originates from the wagging of −OH and the rotation of −CHOH, as shown in Figure 2E. The experimental absorption peak at 2.32 THz is absent in the simulated spectrum, which may be caused by the difference between the experiment and simulation temperatures. Finally, the experimental absorption peak at 2.56 THz corresponds to the simulated absorption peak at 2.51 THz; this peak is attributed to a slight rotation of the six-membered ring and the wagging of −CHOH, as shown in Figure 2F.

The crystal cell structure of α-lactose hydrate is shown in Figure 3A; it is a monoclinic structure with the $P2_1$ (4) chiral space group. The structural parameters are $a$ = 4.7830 (5) Å, $b$ = 21.540 (2) Å, $c$ = 7.7599 (8) Å, $\alpha = 90°$,

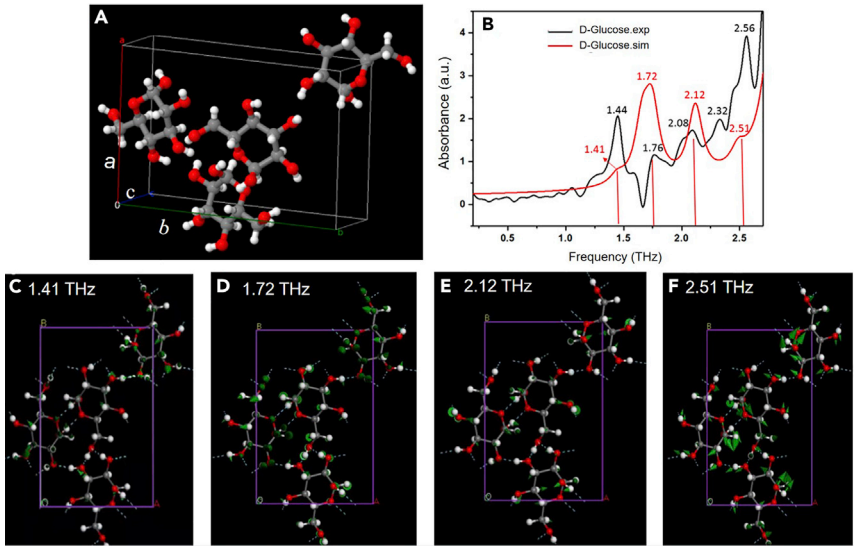


**Figure 2. Simulated results of the THz spectrum and the corresponding vibrational modes of D-glucose**

(A) Crystal cell structure of D-glucose and periodic boundary conditions used in the calculation.

(B) Experimental and simulated THz spectra of D-glucose.

(C–F) Simulated vibrational modes of D-glucose at (C) 1.41, (D) 1.72, (E) 2.12, and (F) 2.51 THz.

$\beta$ = 105.9°, and $\gamma$ = 90°. The simulated and experimental absorption characteristics of α-lactose hydrate in the THz band are shown in Figure 3B, whereas its vibrational modes in different THz bands are shown in Figures 3C–3F. The experimental absorption peak of α-Lactose hydrate at 0.52 THz is not present in the simulated spectrum, which may be caused by the difference between the experiment and simulation temperatures. The experimental absorption peak of α-lactose hydrate at 1.37 THz corresponds to the simulated peak at 1.37 THz; this peak originates predominantly from the collective vibration of α-lactose hydrate molecules, as shown in Figure 3C. The experimental absorption peak at 1.79 THz corresponds to the simulated

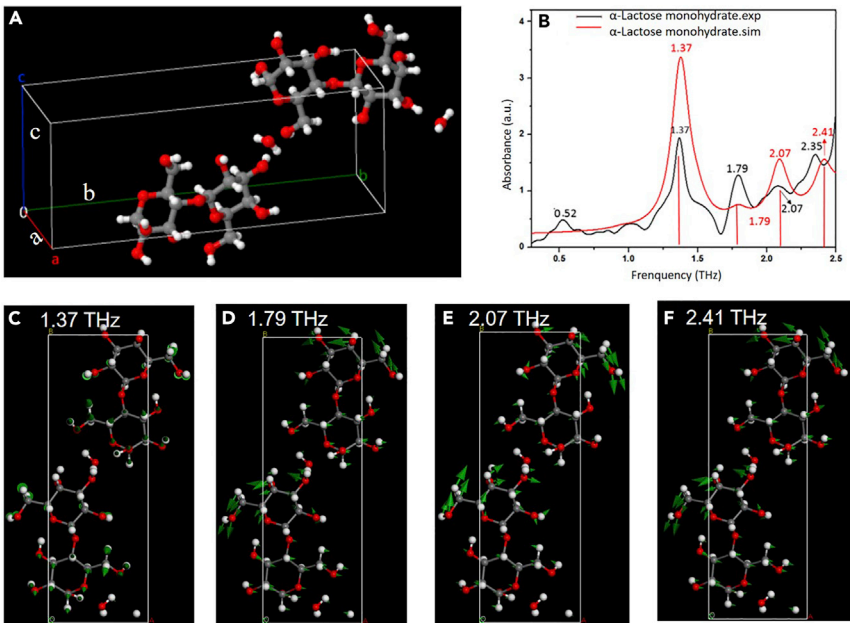


**Figure 3. Simulated results of the THz spectrum and the corresponding vibrational modes of α-lactose hydrate**

(A) Crystal cell structure of α-lactose hydrate and periodic boundary conditions used in the calculation.

(B) Experimental and simulated THz spectra of α-lactose hydrate.

(C–F) Simulated vibrational modes of α-lactose hydrate at (C) 1.37, (D) 1.79, (E) 2.07, and (F) 2.41 THz.

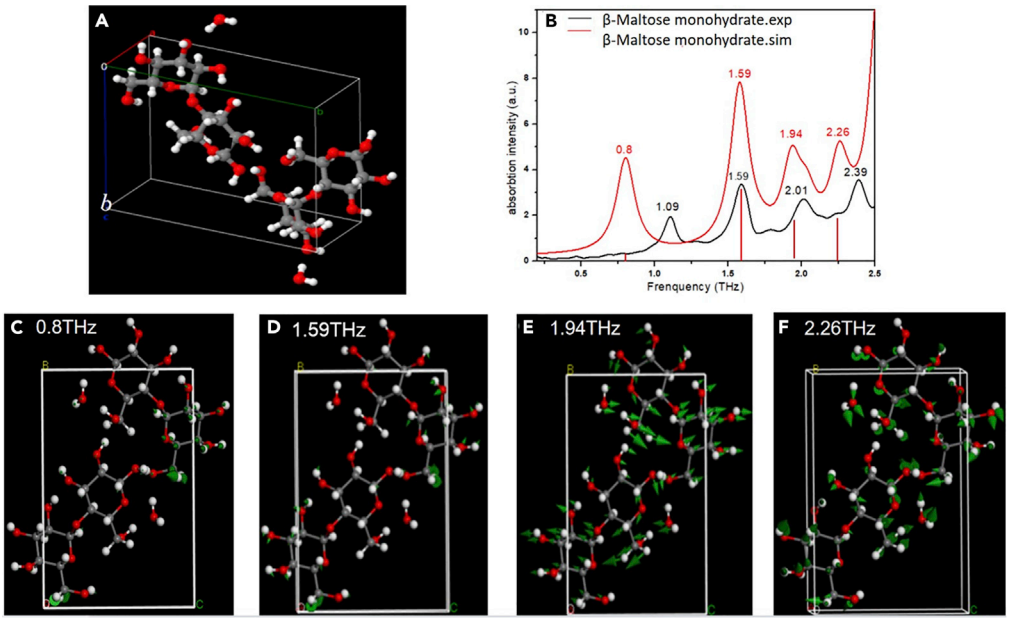


**Figure 4. Simulated results of the THz spectrum and the corresponding vibrational modes of β-maltose hydrate**

(A) Crystal cell structure of β-maltose hydrate and periodic boundary conditions used in the calculation.

(B) Experimental and simulated THz spectra of β-maltose hydrate.

(C–F) Simulated vibrational modes of β-maltose hydrate at (C) 0.8, (D) 1.59, (E) 1.94, and (F) 2.26 THz.

absorption peak at 1.79 THz; this peak arises from the collective translation of α-lactose hydrate molecules, as shown in Figure 3D. The experimental absorption peak at 2.07 THz corresponds to the simulated absorption peak at 2.07 THz; this peak is predominantly due to the translation of the six-membered ring as well as the rotation of −CHOH and −COOH, as shown in Figure 3E. The experimental absorption peak at 2.35 THz corresponds to the simulated absorption peak at 2.41 THz; this peak is predominantly attributed to the rotation of −CHOH, $-CH_2OH$, −OH, and water molecules, as shown in Figure 3F.

The crystal cell structure of β-maltose hydrate is shown in Figure 4A; its crystal structure parameters are $a = 4.866$ (2) Å, $b = 15.077$ (6) Å, $c = 10.702$ (5) Å, $\alpha = 90°$, $\beta = 97.07°$, and $\gamma = 90°$. Its structure is monocline and has the $P2_1$ (4) chiral space group. The simulated and experimental absorption characteristics of β-maltose hydrate in the THz band are shown in Figure 4B. This figure shows that the simulated absorption peaks are consistent with those obtained experimentally. However, there are some deviations and differences between the simulation results and the experimental results, which may also be due to the differences between the simulation and experimental conditions. The vibrational modes of β-maltose hydrate in different THz bands are shown in Figures 4C–4F. The experimental absorption peak at 1.09 THz corresponds to the simulated absorption peak at 0.8 THz; this peak is predominantly due to the intermolecular interaction as well as the rotation of $-CH_2OH$, the six-membered ring, and −OH, as shown in Figure 4C. The experimental absorption peak at 1.59 THz corresponds to the simulated absorption peak at 1.59 THz; this peak predominantly originates from the rotation of $-CH_2OH$ and −OH, as shown in Figure 4D. The experimental absorption peak at 2.09 THz corresponds to the simulated absorption peak at 1.94 THz; this peak is predominantly attributed to the rotation of $-CH_2OH$, −CHOH, −OH, and the six-membered ring as well as the vibration of water molecules, as shown in Figure 4E. The experimental absorption peak at 2.39 THz corresponds to the simulated absorption peak at 2.26 THz; this peak arises from the collective vibration of the β-maltose hydrate molecules, as shown in Figure 4F. The detailed descriptions of vibrational modes of the three saccharides are presented in Table 1.

## THz spectra of the three saccharide solutions

Because most saccharides play a role in the life activities of organisms in the form of solutions, the THz-TDS system was used to measure the liquid samples of the three saccharides in the microfluidic chip. To make the comparison easier, the solid and liquid THz spectra of the three saccharides are illustrated together in Figures 5–7. As shown in Figures 5A and 5B, the absorption peaks of solid D-glucose at 1.44, 1.76, 2.08, 2.32, and 2.56 THz correspond to those of liquid D-glucose at 1.52, 1.71, 2.03, 2.27, and 2.47 THz,

**Table 1. Comparison of the positions of the absorption peaks obtained from the experiments and simulations**

| Sample | Exp liquid (THz) | Exp solid (THz) | Cal (THz) | Vibrational mode description |
|---|---|---|---|---|
| D-glucose | 0.2 | 0.08 | – | – |
| | 0.52 | 1.44 | 1.41 | molecular collective vibration, intermolecular interaction |
| | 1.72 | 1.76 | 1.72 | r (six-membered ring), w (−CHOH, $-CH_2OH$, −OH) |
| | 2.03 | 2.08 | 2.12 | w (−OH), r (−CHOH) |
| | 2.27 | 2.32 | – | – |
| | 2.47 | 2.56 | 2.51 | r (six-membered ring), w (−CHOH) |
| α-lactose monohydrate | 0.19 | 0.13 | – | – |
| | 0.54 | 0.52 | – | – |
| | 1.35 | 1.37 | 1.37 | molecular collective vibration |
| | 1.75 | 1.79 | 1.79 | molecular collective translation |
| | 1.9 | – | – | – |
| | 2.01 | 2.07 | 2.07 | t (six-membered ring),r (−CHOH, $-CH_2OH$) |
| | 2.13 | – | – | – |
| | 2.35 | 2.35 | 2.41 | r (−CHOH, $-CH_2OH$, −OH, $H_2O$) |
| β-maltose monohydrate | 0.16 | 0.12 | – | – |
| | – | 1.09 | 0.8 | r (–$CH_2OH$, six-membered ring, −OH), intermolecular interaction |
| | 1.61 | 1.59 | 1.59 | r (−$CH_2OH$, −OH) |
| | 1.74 | – | – | – |
| | 1.87 | – | – | – |
| | 2.01 | 2.01 | 1.94 | r (–$CH_2OH$, −CHOH, six-membered ring, −OH, $H_2O$) |
| | 2.24 | 2.39 | 2.26 | molecular collective vibration |

The abbreviations adopted for the vibrations are r (Rotation), w (wagging), and t (translation).

respectively. As shown in Figures 6A and 6B, the absorption peaks of solid α-lactose hydrate at 0.52, 1.37, 1.79, 2.07, and 2.35 THz correspond to those of liquid α-lactose hydrate at 0.54, 1.35, 1.75, 2.01, and 2.35 THz, respectively. The absorption peaks of liquid α-lactose hydrate at around 1.90 and 2.13 THz do not correspond to those of solid α-lactose hydrate; this is because water molecules in the solution produce hydrogen bonds, which absorb THz waves and generate absorption peaks (Bosma et al., 1993). As shown in Figures 7A and 7B, the absorption peaks of solid β-maltose hydrate at 1.59, 2.01, and 2.39 THz

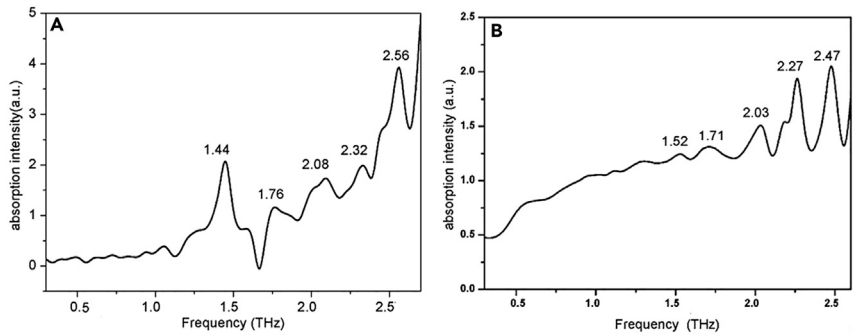


**Figure 5. THz transmission absorption spectra of solid D-glucose and liquid D-glucose**
(A) Solid D-glucose.
(B) Liquid D-glucose.

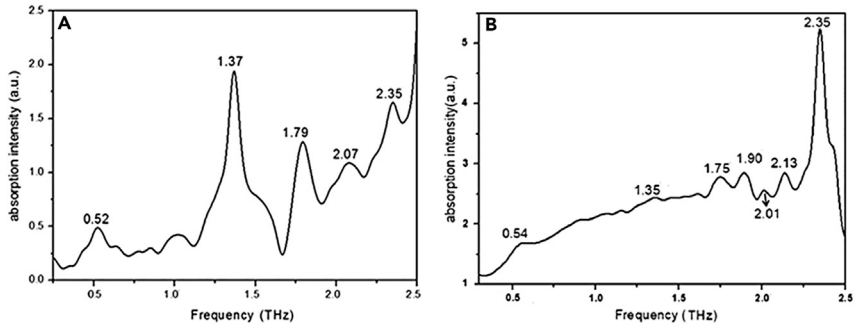


**Figure 6. THz transmission absorption spectra of solid α-lactose hydrate and liquid α-lactose hydrate**

(A) Solid α-lactose hydrate.

(B) Liquid α-lactose hydrate.

correspond to those of liquid β-maltose hydrate at 1.61, 2.01, and 2.24 THz, respectively. The absorption peak of solid β-maltose hydrate at 1.09 THz is not present in the spectrum of the corresponding aqueous solution. This is because, in the aqueous solution, the distance between molecules increases and the intermolecular force decreases. Thus, there is no absorption peak at 1.09 THz in the β-maltose hydrate aqueous solution. Liquid β-maltose hydrate has absorption peaks at 1.74 and 1.87 THz, whereas solid β-maltose hydrate has no absorption peaks at these frequencies. The absorption peaks of liquid β-maltose hydrate may be due to the interaction between β-maltose hydrate and water molecules.

## Conclusion

In this study, the THz spectra of solid D-glucose, solid β-maltose hydrate, and solid α-lactose hydrate were measured, and it was found that the three saccharides have different THz absorption peaks. To verify the accuracy of the experimental results, the solid-state DFT of the Materials Studio quantum chemistry calculation software was used to simulate the intermolecular vibrations of the three saccharides in the THz range. The experimental results are in good agreement with the simulation results. The characteristic absorption peaks of the three saccharides are due to hydrogen bond and intramolecular and intermolecular interactions. Furthermore, the spectral characteristics of the three saccharides were measured in aqueous solutions, and it was found that the THz spectra of the same saccharides in the solid state and aqueous solution are strongly correlated. These results provide the basic spectral properties of D-glucose, α-lactose hydrate, and β-maltose hydrate in the far-infrared THz region and are helpful to understand the low-frequency vibrations of monosaccharides and disaccharides. Thus, our findings provide theoretical guidance for the identification and research of other biological macromolecules.

## Limitations of the study

In this study, the experimental results are roughly consistent with the simulation results, but there are also small differences and offsets. The specific reasons for these differences and offsets need further experimental research.

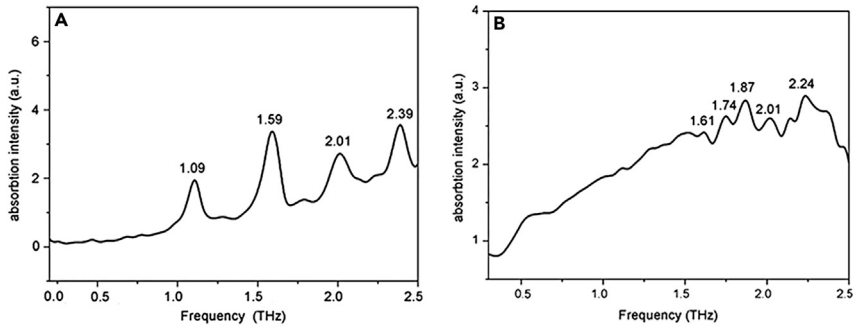


**Figure 7. THz transmission absorption spectra of solid β-maltose hydrate and liquid β-maltose hydrate**

(A) Solid β-maltose hydrate.

(B) Liquid β-maltose hydrate.

## STAR★METHODS

Detailed methods are provided in the online version of this paper and include the following:

- KEY RESOURCES TABLE
- RESOURCE AVAILABILITY
  - Lead contact
  - Materials availability
  - Data and code availability
- EXPERIMENTAL MODEL AND SUBJECT DETAILS
- METHOD DETAILS
  - Experimental setup
  - Sample preparation
  - Fabrication of the microfluidic chip
  - Computational method
- QUANTIFICATION AND STATISTICAL ANALYSIS
- ADDITIONAL RESOURCES

## SUPPLEMENTAL INFORMATION

Supplemental information can be found online at https://doi.org/10.1016/j.isci.2022.104102.

## ACKNOWLEDGMENTS

This work is supported by the National Key R&D Program of China (Grant No .2021YFB3200100) and National Natural Science Foundation of China (NSFC) (61575131). The author thanks Professor Guozhong Zhao for his contribution to sample preparation.

## AUTHOR CONTRIBUTIONS

The academic idea of this study was proposed by Bo Su. The experiment is guided by Cunlin Zhang. Haiyun Huang and Ping Ye carried out the experimental work. Siyu Shao and Guoyang Wang conducted experiment records. The manuscript was written by Haiyun Huang.

## DECLARATION OF INTERESTS

The authors declare no competing interests.

Received: November 23, 2021
Revised: February 28, 2022
Accepted: March 14, 2022
Published: April 15, 2022

## REFERENCES

Banh, A., Bantseev, V., Choh, V., Moran, K.L., and Sivak, J.G. (2006). The lens of the eye as a focusing device and its response to stress. Prog. Retin. Eye Res. *25*, 189–206. https://doi.org/10.1016/j.preteyeres.2005.10.001.

Bosma, W.B., Fried, L.E., and Mukamel, S. (1993). Simulation of the intermolecular vibrational spectra of liquid water and water clusters. J. Chem. Phys. *98*, 4413–4421. https://doi.org/10.1063/1.

Calegari, G.C., Santos, V.A.Q., Teixeira, S.D., Barbosa-Dekker, A.M., and Da Cunha, M.A.A. (2017). Sulfonation of (1→6)-β-D-glucan (lasiodiplodan) and its antioxidant and antimicrobial potential. J. Pharm. Pharmacol. *5*, 850–863. https://doi.org/10.17265/2328-2150/2017.12.002.

Clark, S.J., Segallii, M.D., Pickardii, C.J., Hasnipiii, P.J., and Probertiv, M. (2005). First principles methods using castep. Z. für Kristallographie-Crystalline Mater. *220*. https://doi.org/10.1524/zkri.220.5.567.65075.

Clothier, R.H., and Bourne, N. (2003). Effects of THz exposure on human primary keratinocyte differentiation and viability[J]. J. Biol. Phys. *29*, 179–185. https://doi.org/10.1023/A:1024492725782.

Grimme, S. (2010). Semiempirical GGA-type density functional constructed with a long-range dispersion correction. J. Comput. Chem. *27*, 1787–1799. https://doi.org/10.1002/jcc.20495.

Han, K., Nguyen, T.K., and Park, I. (2010). Terahertz yagi-uda antenna for high input resistance. J. Infrared Millim. Terahertz Waves *31*, 441–454. https://doi.org/10.1007/s10762-009-9596-1.

Klein, H., Belov, S.P., and Winnewisser, G. (1996). Terahertz spectrum of trioxane. Z. Für Naturforschung A *51*. https://doi.org/10.1515/zna-1996-1-218.

Kumar, M., Rajouria, S.K., and Kumar, K.K.M. (2013). Effect of pulse slippage on beat wave THz generation in a rippled density magnetized plasma. J. Phys. D Appl. Phys. *46*, 699–704. https://doi.org/10.1088/0022-3727/46/43/435501.

Li, Z., Hao, Y.H., and Peng, R.Y. (2014). Advances in the biological effects of terahertz wave radiation. Mil. Med. Res. *1*, 129–132. https://doi.org/10.1186/s40779-014-0026-x.

Liu, H., Kurtoglu, M., Cao, Y., Xi, H., and Lampidis, T.J. (2013). Conversion of 2-deoxyglucose-induced growth inhibition to cell death in normoxic tumor cells. Cancer Chemother.

Pharmacol. *72*, 251–262. https://doi.org/10.1007/s00280-013-2193-y.

Liu, W., Liu, Y.B., Huang, J.B., Huang, G.B., Zhang, Y.B., and Fu, W.B. (2018). Application of terahertz spectroscopy in biomolecule detection. Front. Lab. Med. *2*, 127–133. https://doi.org/10.1016/j.flm.2019.05.001.

Mclellan, J.S., Ray, W.C., and Peeples, M.E. (2013). Structure and Function of Respiratory Syncytial Virus Surface Glycoproteins (Springer). https://doi.org/10.1007/978-3-642-38919-1-4.

Nishizawa, J.I., Sasaki, T., and Tanno, T. (2008). Coherent terahertz-wave generation from semiconductors and its applications in biological sciences. J. Phys. Chem. Sol. *69*, 693–701. https://doi.org/10.1016/j.jpcs.2007.07.109.

Perdew, J.P., Burke, K., and Ernzerhof, M. (1998). Generalized gradient approximation made simple. Phys. Rev. Lett. *77*, 3865–3868. https://doi.org/10.1103/PhysRevLett.77.3865.

Sahud, M.A., Caulfield, M., Clarke, N., Koch, R., and Aster, R. (2013). Acute thrombocytopenia in patients treated with amiodarone is caused by antibodies specific for platelet membrane glycoproteins. Br. J. Haematol. *163*, 260–267. https://doi.org/10.1111/bjh.12521.

Selvarajan, E., and Mohanasrinivasan, V. (2015). Kinetic studies on exploring lactose hydrolysis potential of β galactosidase extracted from Lactobacillus plantarum HF571129. J. Food Sci. Tech. *52*, 1–12. https://doi.org/10.1007/s13197-015-1729-z.

Upadhya, P.C., Shen, Y.C., Davies, A.G., and Linfield, E.H. (2004). Far-infrared vibrational modes of polycrystalline saccharides. Vib. Spectrosc. *35*, 139–143. https://doi.org/10.1016/j.vibspec.2003.12.010.

Walther, M., Plochocka, P., Fischer, B.M., Helm, H., and Jepsen, P.U. (2010). Collective vibrational modes in biological molecules investigated by terahertz time-domain spectroscopy. Biopolymers *67*, 310–313. https://doi.org/10.1002/bip.10106.

Wang, W.A., Liu, W., Yang, X., and Liu, Y.W. (2016). Terahertz time-domain spectroscopy of anhydrous glucose. Chin. J. Lasers *43*, 241–248. https://doi.org/10.3788/CJL201643.1111001.

Whiteside, P.T., Shen, Y.L., Madden-Smith, C.E., Turner, P., Patel, N., and George, M.W. (2008). Detection of low levels of amorphous lactose using H/D exchange and FT-Raman spectroscopy. Pharm. Res. *25*, 2650–2656. https://doi.org/10.1007/s11095-008-9682-4.

Xu, Z., Lv, X., Chen, J., Jiang, L., Lai, Y., and Li, J. (2016). Dispersion-corrected dft investigation on defect chemistry and potassium migration in potassium-graphite intercalation compounds for potassium ion batteries anode materials. Carbon *107*, 885–894. https://doi.org/10.1016/j.carbon.2016.06.101.

Zheng, Z.P., Fan, W.H., Liang, Y.Q., and Hui, Y. (2012). Application of terahertz spectroscopy and molecular modeling in isomers investigation: glucose and fructose. Opt. Commun. *285*, 1868–1871. https://doi.org/10.1016/j.optcom.2011.12.016.

## STAR★METHODS

### KEY RESOURCES TABLE

| REAGENT or RESOURCE | SOURCE | IDENTIFIER |
|---|---|---|
| D-Glucose | J&K Chemical | CAS#: 50-99-7 |
| α-Lactose hydrate | J&K Chemical | CAS#: 5989-81-1 |
| β-Maltose hydrate | J&K Chemical | CAS#: 6363-53-7 |
| D-Glucose crystal | Cambridge Crystallographic Data Center | CAS#: 50-99-7 |
| α-Lactose hydrate crystal | Cambridge Crystallographic Data Center | CAS#: 5989-81-1 |
| β-Maltose hydrate crystal | Cambridge Crystallographic Data Center | CAS#: 6363-53-7 |
| Software and algorithms | | |
| Origin 8 | Origin Lab | https://www.originlab.com/ |
| Materials Studio | Castep | http://www.castep.org/ |
| Deposited data | | |
| Data | This paper | https://doi.org/10.5281/zenodo.6351093 |

### RESOURCE AVAILABILITY

#### Lead contact

Further information and requests for resources and reagents should be directed to and will be fulfilled by the Lead Contact, Bo Su (subo75@cnu.edu.cn).

#### Materials availability

This study did not generate new unique reagents.

#### Data and code availability

All data has been deposited at Zenodo (Huang et al., 2022) and is publicly available as of the date of publication. DOI are listed in the key resources table.

This paper does not report original code.

Any additional information required to reanalyze the data reported in this working paper is available from the lead contact upon request (subo75@cnu.edu.cn).

### EXPERIMENTAL MODEL AND SUBJECT DETAILS

Our study does not use experimental models typical in the life sciences.

### METHOD DETAILS

#### Experimental setup

Our experimental setup comprises an ordinary THz-TDS system. The central wavelength of the femtosecond laser is 800 nm, the pulse width is 100 fs, the output power is 0.9 W, and the pulse repetition rate is 80 MHz. The spectral width of THz-TDS system is 0.1– 2.5 THz. After passing through the beam splitter, the femtosecond laser is divided into two beams. One is the pump beam, which is focused on an InAs crystal through an electric translation stage and a lens to generate THz pulses. THz waves converge on the sample after collimating with an off-axis paraboloid mirror. The THz wave containing the sample information is focused on the ZnTe crystal through another off-axis paraboloid mirror, and the crystal is electro-optically modulated to change its refractive index. At the same time, the probe linearly polarized laser changes into elliptically polarized light after passing through the electro-optic crystal with changed refractive index. After the elliptically polarized light passes through a quarter wave plate and Wollaston prism, two unequal orthogonal polarized beams are generated and detected by the differential detector. The differential photocurrent detected by a differential detector is not zero. The magnitude of this differential current is directly proportional to the THz electric field. Therefore, the time domain waveform of the THz pulse can be obtained according to the magnitude of the differential current. During the experiment, the relative

optical path difference between THz pulse and detection light is adjusted using a computer-controlled electric translation table, and the entire time-domain waveform of the THz pulse is obtained via point-by-point scanning. The experimental light path is shown in Figure S1.

### Sample preparation

Solid D-Glucose (monosaccharide), α-Lactose hydrate (disaccharide), and β-Maltose hydrate (disaccharide) were prepared using the tablet pressing method. First, each sample and polyethylene were mixed in a mass ratio of 1:1 and fully ground. The mixture was then pressed by applying a pressure of 3 t to obtain flake samples with a diameter of 1.2 cm and a thickness of 1 mm. The concentrations of the aqueous solutions of the three saccharides were 0.5, 0.1, and 0.5 g/mL, respectively.

### Fabrication of the microfluidic chip

The strong absorption of THz waves in water makes it difficult to study liquid samples via THz spectroscopy. The microfluidic technology reduces the absorption of THz waves in water by reducing the distance between the liquid samples and the THz waves, thus increasing the sensitivity of the detected signals. The microfluidic chip comprises organic glass and the COC5013 material with high transmittance to THz waves. As COC5013 is expensive and difficult to obtain, we used COC5013 only for the THz detection area of the microfluidic chip, and organic glass was used for preparing other areas of the chip. First, a 12 mm long, 8 mm wide and 2 mm high organic glass was prepared. A 6 mm long, 5 mm wide and 2 mm high rectangular hole was cut in the middle of the organic glass using a laser engraving machine. Then, two 700 μm vertical intersecting liquid channels were drilled at the left and right positions of the organic glass using the spot shooting function of the laser engraving machine. Second, the COC5013 material was cut to the same size as the rectangular hole on the organic glass. A channel with a length of 6 mm, a width of 3.5 mm, and a height of 0.3 mm milled on the left-and right-hand sides of the COC5013 material using a milling cutter; this channel was used as the detection area of the liquid samples. Finally, the COC5013 with the detection area was embedded in the organic glass with liquid inlet and outlet channels, and the gap between the two materials and the end faces of the left and right drill hole on the organic glass were sealed using hot-melt adhesive to avoid liquid leakage. The fabrication process of the microfluidic chip is shown in Figure S2.

### Computational method

To analyze the experimental spectra in detail and explore the specific reasons for the formation of absorption peaks, quantum chemical simulation calculations were performed via the solid-state DFT using the Cambridge Sequential Total Energy Package (CASTEP) program (Clark et al., 2005) as a part of the Materials Studio package from Accelrys. The crystal cells used to calculate the three saccharides were all obtained from the Cambridge Crystallographic Data Centre and the results were obtained for the crystalline state within the generalized gradient approximation (GGA) at Perdew-Burke-Ernzerhof (PBE) (Perdew et al., 1998; Xu et al., 2016) correlation functional. The Grimme's DFT-D2 dispersion corrected method and norm-conserving pseudopotentials were implemented in CASTEP (Grimme, 2010).

## QUANTIFICATION AND STATISTICAL ANALYSIS

There is no statistical analysis in this paper.

## ADDITIONAL RESOURCES

We have no relevant resources.